Library through Editor of Met Mag.

MET O 19 BRANCH MEMORANDUM No. 38

THE EFFECT OF ASSUMPTIONS, EXPERIMENTAL ERRORS AND UNCERTAINTIES IN AEROSOL PHYSICAL PROPERTIES ON THE INTERPRETATION OF LIDAR OBSERVATIONS OF THE STRATOSPHERIC AEROSOL LAYER

by

A. SLINGO, G. J. JENKINS and G. E. HUNT

Met O 19
(High Atmosphere Branch)
Meteorological Office
London Road
BRACKNELL
Berks RG12 2SZ

June 1977

The effect of assumptions, experimental errors and uncertainties in aerosol physical properties on the interpretation of lidar observations of the stratospheric aerosol layer.

1. Introduction

Since the first direct observations of the stratospheric aerosol layer in the early 1960's, the layer has been observed using a variety of direct and indirect techniques, including impactors flown on aircraft, photoelectric counters and coronographs mounted on balloons and ground based searchlights and laser radar (Lidar). These observations have shown that the layer is enhanced by the material injected into the stratosphere by volcanic activity. Following a large volcanic eruption a plume of gas and dust penetrates into the stratosphere, forming a layer a few kilometers thick with a maximum density at about 20 km altitude. Initially, the layer is composed mainly of silicate dust, but this material is removed gradually by settling and mixing into the troposphere, until after about a year the dominant constituent appears to be a polydispersion of droplets of a sulphuric acid/water solution, formed from the sulphur-laden gases in the volcanic plume (for a review see Cadle and Grams, 1975). The general stratospheric circulation ensures that, despite the discrete source, the layer is eventually spread world-wide.

In recent years there has been considerable interest in the radiative properties of such a global layer and in its effect on the earth's climate. A wide range of theoretical models have been constructed, ranging from simple analytical representations to complex radiation schemes, and they suggest that following a major volcanic eruption the layer should produce significant changes in the atmospheric temperature field, ranging from a cooling of up to $1^{\circ}K$ at the surface to an in situ heating of up to about $10^{\circ}K$. These predictions are in agreement with the temperature changes observed following the eruption of Mt Agung in 1963 (e.g. Baldwin et al 1976, Harshvardhan and Cess 1976).

Observations of the stratospheric aerosol layer by laser radar have been made for at least a decade and have contributed significantly to the understanding

of the structure of the layer. In the analysis of data from ground-based lidar, various assumptions as to the physical properties of the aerosol have to be made in order to derive densities and optical depths and to estimate the effect of the observed layer on the climate. In this paper the effect of these assumptions and of experimental errors on the interpretation of the single and two-wavelength observations made at 465 nm and 605 nm with the UK Meteorological Office Lidar (Pettifer et al 1976) will be discussed in detail. Many of the results are not specific to this particular system and illustrate some general limitations on remote sounding using lidar.

2. Analysis of single-wavelength observations

In this section we shall outline the procedure for analysing observations made at a single wavelength and discuss the effect of the assumptions made and of errors on the results. A detailed account of the Lidar and of the basic theory has already been given (Pettifer et al 1976). The number of backscattered photons received from a layer of thickness δz at altitude z, from a single laser pulse is given by;

$$P(z) = \frac{P_o E q_o^2 q^2(z) \delta z (f_p + f_m)}{z^2} \qquad (1)$$

The symbols used in this section are defined in Table 1. In principle, measurement of the other quantities in equation 1 allows the determination of f_p, the aerosol backscatter coefficient. Unfortunately this is not possible directly, as some of these quantities are currently very difficult to measure with the required precision. The parameter which is most difficult to estimate is the receiver sensitivity, E, although there are also serious problems involved in determining the transmission (q_o) of the atmosphere from the ground to the lowest altitude of interest (due to the often large and variable contribution from hydrometeors and dust in the troposphere) and also in monitoring the number of photons in the Lidar pulse, P_o. For these reasons the analysis of single-wavelength Lidar data has always used the 'clean-air' calibration technique (Fiocco and Grams 1964, Russell et al 1976), in which the value of the product $P_o E q_o^2$ is found by assuming that at some level z' within the altitude range covered by the analysis the aerosol content is zero. At this height equation 1 reduces to;

$$P'(z') = \frac{P_o E q_o^2 q^2(z') \delta z f_m}{z'^2} \qquad (2)$$

from which $K = P_o E q_o^2$ can be calculated. For each altitude it is now possible to calculate the backscattered signal expected from the air molecules alone;

$$M(z) = \frac{K q^2(z) \delta z f_m}{z^2} \qquad (3)$$

Dividing equation 1 by equation 3;

$$R(z) = \frac{P(z)}{M(z)} = 1 + \frac{f_p}{f_m} \qquad (4)$$

Therefore, the assumption that at the altitude z' the scattering ratio, $R(z)$ is unity allows the value of f_p to be found for the rest of the profile.

2.1 Errors introduced by the 'clean-air' calibration

It is important to note that the clean-air normalisation will lead to an under-estimate of the aerosol amount if aerosol is in fact present at the normalisation level, z' . From the results of a series of balloon measurements of the layer made at Laramie, by the University of Wyoming group, Russell et al (1975) showed that had Lidar measurements been made at the time of the balloon ascents, the clean-air normalisation technique applied in the height range 10-30 km would have under-estimated the scattering ratios at all altitudes by typically less than 10% of $(R_{max} - 1)$. Normalisation is usually carried out at the lowest possible altitude, where the photon counting statistics are best, but had normalisation been carried out above the peak of the aerosol layer the error would often have been greater. However, in our experience the backscatter ratio at our lowest altitude interval of 10-12 km is often not a minimum, presumably being enhanced by small amounts of cloud present at this altitude (see section 5).

At time of low volcanic activity R_{max} is typically 1.1 or even less at 605 nm, so that the error in $R(z)$ is expected to be less than 0.01 at all altitudes. Although apparently very small, this error would be present at all levels and the effect on the integrated backscatter, which is used to calculate the total amount of aerosol in the stratosphere, could be significant.

As an example, consider the scattering ratio profile (a) illustrated in Fig. 1, which is Gaussian in shape with R_{max} equal to 1.1 at 20 km and with a full width to half maximum of 8 km. An underestimate of 10% of $(R_{max} - 1)$ at every level transforms this curve to (b) and to (c) for an under-estimate of 20% of $(R_{max} - 1)$, which is a more realistic estimate of the possible error when normalisation is carried out above the peak of the layer. The corresponding effect on the backscatter coefficient is shown on the right hand side of Fig. 1. The increases in the integrated backscatter coefficient for the layer are 36% and 72% respectively. These are much

larger than the percentage increases in the scattering ratios, due to the increased contribution from the lowest altitudes, for which a given scattering ratio corresponds to a much larger backscatter coefficient than at greater altitudes because of the increase in air density.

2.2 Errors in calculating the molecular backscatter coefficient (β_m)

A knowledge of the altitude profile of the molecular number density is required in order to calculate the molecular backscatter coefficient, which is simply the product of the number density and the Rayleigh backscatter cross section for the normal atmospheric composition. Our Lidar observations of stratospheric aerosols are always made at night. Number density data are obtained from the midnight radiosonde ascent from Crawley, which is about 55 km to the south-east of the Beaufort Park experimental site. The geographical separation of the two sites is small enough to ensure that the number density profile is representative of the atmosphere above the Lidar. It is important, however, to use the radiosonde data for the night of the Lidar run; use of data from the previous or following nights can lead to errors of 100% in ($R(z)-1$) in the quickly changing synoptic situations so typcial in England in the winter months. Use of data from a climatological profile instead of from a radiosonde can also lead to large errors.

Errors in the radiosonde data are difficult to assess. Comparisons between sondes of the same and different types have been made in order to estimate systematic and random errors and they suggest that in the stratosphere the errors in the derived number densities are small and are here assumed to be a nominal one percent (Harrison 1962, Lenhard 1973).

2.3 Errors in the atmospheric transmission

As the laser pulse passes through the stratosphere it is attenuated by scattering and absorption by the gaseous and aerosol components of the atmosphere. Failure to take account of this attenuation leads to a small but significant distortion of the scattering ratio profile. The total attenuation is low, amounting to only about 5 per cent from 10 km to 30 km, except at times of exceptional aerosol loading, and the error introduced into the scattering ratio is less than 1 per cent.

Rayleigh scattering is taken into account using the transmissions tabulated in the Handbook of Geophysics and Space Environments (Valley, 1965). These data were interpolated to derive the transmissions at the laser operating wavelengths of 465 and 605 nm. Absorption due to ozone is important only at 605 nm which is almost coincident with the peak of the Chappuis band. The variability in the amount of ozone present in the stratosphere is taken into account using the daily measurements of total ozone by the Dobson spectrophotometer at Beaufort Park. The effect of absorption by NO_2 is less than 0.5% at 465 nm and has been ignored.

No allowance is made for the attenuation of the beam by scattering from the aerosols themselves, as at the present time this is much less important than Rayleigh scattering and gaseous absorption. At times of large aerosol densities, such as in 1963 following the eruption of Gunung Agung, the scattering ratio profile would have to be corrected for aerosol scattering using an iterative procedure.

2.4 Pulse counting errors

The Lidar receiving system is operated in the photon counting mode and counts are corrected for the sky background and for the pulse pile-up phenomenon, as described by Pettifer et al (1976). The contribution to the experimental error in the scattering ratio from photon counting statistics produces an uncertainty of typically 0.3 per cent at 11 km, rising to 3-4 per cent at 29 km, for the usual length of run of about two hours.

2.5 Summary of errors

Table 2 shows how the errors described above vary as a function of altitude and how they contribute to the error in the Scattering Ratio. The radiosonde density errors, transmission errors and the photon counting errors are combined assuming them to be uncorrelated variables. To illustrate the results of such an analysis, Figure 2 presents the data received at 465 nm on the night of 23-24 November 1976. It will be seen that the stratosphere is very 'clean' at the present time, with particulate backscattering less than 10 per cent of the molecular backscatter in the visible.

3. Aerosol radiative properties

Having derived the altitude profile of the scattering ratio, and hence of the aerosol backscatter coefficient f_p it is necessary to assume a model for the aerosol in order to calculate number densities and to assess the impact on the earth's climate. The optical thickness of the aerosol layer is assumed to be sufficiently small for multiple scattering to be ignored. This assumption is a very good one which only begins to break down at times of heavy aerosol loading on the stratosphere. The aerosols are taken to be spherical in shape, which is supported by in situ sampling (Cadle and Grams 1975). Mie scattering theory can therefore be used to calculate the radiative properties of the aerosol. The backscattered intensity from irregularly shaped particles has been found to be lower than that predicted by Mie theory (Holland and Gagne, 1970), although the intensity will obviously be very much a function of the precise shape and orientation of the particles. A computer programme was used to carry out the Mie calculations. The input data are the wavelength of the incident radiation and the complex refractive index and size distribution function (and hence number density) of the aerosol particles. The last two quantities have to take assumed values in the calculation and in this section we examine how the uncertainty in the knowledge of these values affects the derived aerosol properties.

3.1 Calculations

The volume extinction and scattering cross sections, β_{EXT} and β_{SCAT}, are computed first, from which the optical depth, τ_λ, may be found by integration along the line of sight;

$$\tau_\lambda = \int_{z_1}^{z_2} \beta_{EXT}(z)\, dz \qquad (5)$$

The single-scattering albedo, ω_λ, is the fraction of the radiation which is scattered in an interaction;

$$\omega_\lambda = \frac{\beta_{SCAT}}{\beta_{EXT}} \qquad (6)$$

The phase function, $p(\mu, -\mu')$, where μ and μ' are the direction cosines of the incident and scattered radiation, respectively, describes the angular dependence of the scattered radiation intensity (for a full

discussion of these parameters see Deirmendjian (1969) and Hunt (1971). The backscatter coefficient is then given by;

$$f_p = \beta_{SCAT} \cdot \frac{P(1,-1)}{4\pi} \tag{7}$$

For a global stratospheric aerosol layer the fraction of the incident solar power scattered away from the earth is given by the spherical albedo;

$$R_\lambda = \tau_\lambda \int_0^1 d\mu \int_0^1 d\mu' P(\mu,-\mu') \tag{8}$$

The absorptivity of the layer is given by;

$$A_\lambda = 2\tau_\lambda (1-\omega_\lambda) \tag{9}$$

In order to calculate the influence of the aerosol layer on the solar beam it is necessary to integrate these radiative properties over the wavelength distribution of solar radiation, which is approximated by the Planck function for a 6000 K black body, with a cut-off below 0.3 μm to take account of absorption by ozone above the aerosol. This procedure was carried out using eleven wavelengths between 0.3 μm and 2.4 μm to derive the "flux-weighted" values of the optical depth, τ, the absorptivity, A, and the spherical albedo, R. The error introduced into the flux-weighted values by the use of only eleven wavelengths in the representation of the solar spectrum is less than one per cent.

These calculations allow the observed backscatter coefficient to be related to the aerosol number density and optical depth, which may be used to compare Lidar results with those of other instruments. The derived values of τ, A and R may also be used in simple climate models to assess the climatic impact of the aerosol layer. The purpose here is to assess how uncertainties in the knowledge of the assumed aerosol physical properties affect the predicted climatic perturbation. The radiative energy balance model of Coakley and Grams (1976) will be used. In this model the interaction of the aerosol with both solar and terrestrial radiation fields is computed for a global stratospheric aerosol layer, radiative equilibrium being

maintained both at the top and bottom of the stratosphere. From the work of Coakley and Grams (1976) and others, the perturbation brought about by aerosols is mainly due to modification of the solar radiation field, so we shall ignore the contribution from the terrestrial radiation field. In this case the model gives a simple expression for the predicted change in global mean surface temperature;

$$\Delta T_s = -100\left\{\frac{A}{2}\cdot\frac{(1-3\alpha)}{(1-\alpha)} + R(1-\alpha)\right\} \qquad (10)$$

where α is the planetary albedo, taken to be 0.3 (Raschke et al 1973).

3.2 Results

The results of these calculations are illustrated in Figs 3-6 and in Table 3. In Figs 3-5 a wide range of values of the real and imaginary parts of the refractive index have been used to derive f_p , τ and ΔT_s , the size distribution function being the commonly used Haze H function (Deirmendjian, 1969). This is a "modified gamma distribution" defined by;

$$\frac{d\,n(r)}{d\log r} = C r^{1+a} \exp\left(-b r^{\gamma}\right) \qquad (11)$$

where r is the particle radius and the mode radius, r_c , which is the radius of maximum frequency in the distribution, is found from;

$$b = \frac{a}{\gamma r_c^{\gamma}} \qquad (12)$$

For the Haze H function $\gamma = 1$, $a = 2$, $r_c = 0.1\,\mu m$, hence $b = 20$.

The integrated particulate backscatter mentioned in Figures 4 and 5 is obtained by vertical integration of the observed backscatter coefficient profile and is therefore measured in sr^{-1} . The range of refractive indices which have been used in calculations relating to stratospheric aerosols is indicated approximately on these figures by the dashed lines. The most persistent constituent is a 75% sulphuric acid/25% water solution,

for which in the visible part of the spectrum the real refractive index is 1.43, but in the first few months following a major volcanic eruption, silicate material, which has a real refractive index of about 1.56, is sometimes a major constituent, while values as low as 1.4 have been used in calculations (Cadle and Grams 1975).

It will be noted from Figure 3 that number densities derived from Lidar backscatter observations at 0.605 /um vary by a factor of about three, depending on the refactive index chosen, while the derived optical depth and predicted surface temperature reduction vary by a factor of about two. At 465 nm the sensitivity of these parameters to the refractive index is slightly greater. At times where there is uncertainty as to the fraction of non-sulphuric acid aerosols present in the stratosphere, the interpretation of Lidar data is therefore very dependent on the refractive index chosen and the uncertainties in the derived properties can be much larger than the experimental errors in the Lidar data themselves.

Data on the size distribution function of stratospheric aerosols have been summarised by Toon and Pollack (1976) and by Bigg (1976), who derived the variability with altitude and season. To find the effect of different size distributions on the radiative properties the five model distributions illustrated in Figure 6, which reflect the variability found by Bigg, have been used. All are modified gamma distributions and include the Haze H function used earlier. The functions are normalised so that in the size range 0.01 /um to 2 /um there are 1 particles per cubic centimetre. The properties of aerosol populations with these distributions were calculated for a refractive index of 1.5 - 0.001 i, which lies in the centre of the expected refractive index range so as to give a representative dependence on size distribution.

The results are summarised in Table 3. The large spread in the backscatter coefficients is due to the fact that the number densities are normalised over a radius interval which extends well below the minimum optically important size of about 0.1 /um, so that a distribution with a sharp cut-off above this radius, such as that with $\gamma = 0.3$, produces much

smaller backscatter coefficients than the others. This illustrates how sensitive derived number densities are to the size distribution and size interval.

The rest of Table 3 shows that at 605 nm the derived optical depth and predicted surface temperature decrease can vary by a factor of over two, depending on the size distribution chosen, the dependence being less at the shorter wavelength. The function with $\gamma = 0.2$, for example, which corresponds to Bigg's data for the lower stratosphere (10-16 km) in Spring, produces much lower values of τ and ΔT_s for a given observed particulate backscatter than the Haze H function.

For the scattering ratio profile illustrated in Figure 2, the value of the integrated backscatter is $1.9.10^{-4}$ sr^{-1}. Assuming the aerosol size distribution to be represented by the Haze H function and the refractive index to be 1.5 - 0.001 i, the first line in Table 3 allows the optical depth and predicted temperature change to be found. These are 0.0050 and -0.16 K respectively, which illustrates the minor role of the background aerosol at the present time as a contributor to climatic change.

4. Analysis of Lidar observations at two wavelengths

In the previous sections it has been shown that the analysis of single-wavelength Lidar data is hampered by the necessity to make three basic assumptions about the aerosol, all of which could lead to large systematic errors. The first assumption is that there is an aerosol-free layer at some point in the altitude range of the laser. Values for the refractive index and the size distribution function also have to be assumed in the interpretation of the scattering ratio data. The addition of a second nearly simultaneous sounding allows one of these assumptions to be removed. In this section the two-wavelength technique introduced by Pettifer et al (1976) will be analysed. This technique does not require the assumption of an aerosol-free layer. In the next section a slightly different analysis is examined by which information on the size distribution function can be recovered.

Pettifer's analysis requires only relative values at the two wavelengths of the system efficiency, the transmitted energy and the atmospheric transmission. From the ratio of the number of photons received at the two wavelengths it is then possible to determine the ratio $(f_m + f_p)_{\lambda_1} / (f_m + f_p)_{\lambda_2}$. To interpret this ratio the wavelength dependence of f_p is required, so the physical properties of the aerosol still have to be assumed. The removal of the clean-air normalisation is a very useful step forward, however, and allows a check to be made on the validity of the normalisation technique.

Although the measurement of the relative system efficiencies is less demanding than of the absolute efficiencies, it is still far from being trivial. The problems of determining the relative sensitivity and laser energy need to be considered together, as the parameter which needs to be monitored is the sensible energy of the laser, which is the backscattered energy detected by a receiver of known efficiency. In a tunable system (e.g. a dye laser), unless the laser energy monitor employs a narrowband filter closely matched to that of the receiver, changes in wavelength will result in a misleading estimate of the transmitted energy. Experience with the present system has shown that for an untuned dye laser with the broadband output produced by the Rhodamine 6G dye, both the peak wavelength and the full width at half maximum of the laser pulse vary with dye temperature and age. It is therefore desirable both to stabilise the laser wavelength and to

narrow the pulse width to the point where small wavelength drifts will not produce large changes in transmissions through the narrowband filter. Both of these requirements are met by the addition of an intra-cavity Fabry-Perot interferometer. This would not normally be necessary in the case of, for example, Ruby lasers, unless the filters employed were of very narrow bandwidth. The energy monitor also needs to be insensitive to the polarisation state of the pulse, as the present system uses a mixed-mode laser, for which the characteristic mode and hence the polarisation state may vary from shot to shot. These considerations complicate the determination of the sensitivities and energy monitor calibrations by firing the laser via a known attenuation into the receiver system and noting the relationship between receiver response and energy monitor response, as described by Pettifer et al (1976). Further work is in hand to ensure that they do not adversely affect the experimental results.

When the clean-air normalisation is applied, the atmospheric transmission between the ground and the altitude z_1, does not need to be known. In the two wavelength experiment the relative transmissions are required and this quantity is dominated by the tropospheric contribution. Pettifer and co-workers used the data of Irvine and Peterson (1970) to obtain the climatological average for the ratio of the two transmissions. There is, unfortunately, a tendency for this ratio to increase as the transmission decreases (Fig. 7). Such a variation with transmission is not surprising, however, because of the variability in the relative amounts of aerosol, hydrometeors, etc, in the troposphere and their different wavelength dependent transmissions, but it means that the best estimate of the transmission ratio can only be found if the absolute transmission is also known, which removes one of the advantages of the two wavelength approach. If this dependence is ignored and a climatological value used, the scatter in Irvine and Peterson's data suggests that uncertainties of about 10 per cent in the value of the square of the transmission ratio would result.

An error analysis for the two wavelength experiment has been carried out and the results are presented in Table 4. These calculations assume that the

aerosol has the Haze H size distribution function with a complex refractive index of 1.5 - 0.005 i.

The first column lists the value of the scattering ratio at 605 nm, $R_{605}(z)$, which determines the ratio of the number of backscattered photons received at the two Lidar wavelengths, $P_{605}(z)/P_{465}(z)$. The table then lists the required percentage errors in the photon counts and the ratios of the number of transmitted photons, the receiver efficiencies and the square of the transmissions, in order to produce an error of 100 per cent in the derived optical depth. From the discussion in section 2.4 it will be seen that the accuracy required in the measured count rates can be met over the altitude range of interest. However, the requirement for uncertainties in the other quqntities of only a few per cent is much more difficult to meet. In particular q_o^2 cannot be measured to better than about 10 per cent at the present time. It must be concluded that the clean-air calibration assumption can only be dispensed with at times of exceptional aerosol densities.

5. Two-wavelength runs analysed separately

The simplest way to analyse two-wavelength data is to treat each wavelength run separately, applying the clean-air normalisation at the same altitude, and then calculating two scattering ratio profiles. This allows the additional information provided by the second wavelength to be used to determine the most likely size distribution function, by comparing the ratios of the theoretical backscatter coefficients listed in Table 3 to the observed ratio. The uncertainty in the choice of size distribution function is then determined by the relative sizes of the error in the observed ratio and the spread in the theoretical values. It is necessary to return to the use of the clean-air calibration technique, but in view of the difficulties in applying the analysis outlined in the previous section at times of low aerosol densities this is an acceptable constraint.

As an example of the method of analysis, Fig. 8 shows the Lidar data obtained at 605 nm on the night of November 22-23 1976, which together with the 465 nm data presented in Fig. 2 are analysed in Table 5 to derive values for the ratios of the aerosol backscatter coefficients. The results are unusual in that the wavelength dependence of the aerosol backscatter coefficient is even greater that that of the molecular term. This suggests that in the range 0.1 - 1 μm the size distribution function was much steeper than those shown in Figure 6, although the errors on the value of the observed ratio are large. It is possible that the data for 22-23 November are affected by thin cirrus cloud at the lowest altitude. This would result in scattering ratios which were too low and would explain the unusual wavelength dependence. Because of the potentially much greater backscatter by cirrus than by aerosol, great care has to be taken in using the clean-air normalisation technique at altitudes where even very small amounts of cloud may be present.

This technique will not work if the shape of the actual and model size distribution functions are different. In principle, the use of many operating wavelengths over as wide a wavelength range as possible allows the shape of the size distribution function to be found by inverting the backscatter data directly. However, the small wavelength range available and the blurring effect of the

Mie functions on features in the size distribution function means that such direct methods are of little practical use. This is illustrated by Figure 9, for which the wavelength dependence of the backscatter coefficient over the range 0.3 - 3.3 /um has been calculated for each of the five model distribution functions used previously. These curves have very similar shapes, with no pronounced spectral features, the largest differences in slope occurring at about 0.7 /um. Two operating wavelengths spaced as widely as possible below about 1 /um will therefore provide as much information on the size distribution function as the restricted frequency range available will allow. The only obvious disadvantage of the present system is therefore that the two wavelengths are too close to allow useful size distribution information to be obtained, except at times of high stratospheric aerosol content.

The results still depend, however, on the refractive index assumed and on the clean-air normalisation technique. Additional information on the refractive index could be obtained from measurements at several scattering angles. Such measurements have been made using a Laser polar nephelometer mounted on an aircraft (Grams, Dascher and Wyman, 1975), but the method is most sensitive at scattering angles less than 90°, so that a major re-organisation of the present system would be required to use this configuration.

6. Conclusions

In this paper the steps in the analysis of Lidar observations of the stratospheric aerosol layer which are most sensitive to assumptions and experimental errors have been examined. The most important areas are;

(1) In the analysis of single wavelength data the need to assume that there is no aerosol present at some altitude in order to normalise the data can lead to large errors if aerosol is in fact present. This danger can be reduced by analysing the Lidar signal from as wide an altitude range as possible.

(2) The need to assume that there is an aerosol-free layer can be removed by the addition of a second operating wavelength. Difficulties in determining sufficiently accurate values for the relative receiver sensitivities, laser energies and atmospheric transmissions, however, means that the assumption can only be checked when aerosol densities are high.

(3) At times of low aerosol density the data from the two wavelength runs are best analysed separately, returning to the aerosol-free layer assumption but in principle allowing some information to be recovered on the size distribution function.

(4) Uncertainties in the values for the aerosol refractive index and size distribution function can lead to errors of at least a factor of two in the derived density, optical depth and predicted temperature change. The error due to ignorance of the refractive index will probably be important only immediately following a volcanic eruption, when the proportions of silicate dust and sulphuric acid are unknown. However, there is still only a very limited climatology for the size distribution function, so that errors from this source are always important. Data on aerosol size distributions can be obtained by two-wavelength Lidar systems, provided the operating wavelengths are well spread over the visible window region, although the results would still depend on the restrictions outlined above.

References

Baldwin B., Pollack J.B., Summers A., Toon O.B., Sagan C. and Van Camp W. (1976) "Stratospheric aerosols and climatic change". Nature 263, 551-555.

Bigg E.K. (1976) "Size distributions of stratospheric aerosols and their variations with altitude and time". J. Atmos. Sci. 33, 1080-1086.

Cadle R.D., and Grams G.W. (1975) "Stratospheric aerosol particles and their optical properties". Rev. Geophys. Space. Physics. 13, 475-501.

Coakley J.A. and Grams G.W. (1976) "Relative influence of visible and infrared optical properties of a stratospheric aerosol layer on the global climate". J. Appl. Met. 15, 679-691.

Deirmendjian D. (1969) "Electromagnetic scattering on spherical polydispersions". Elsevier, New York.

Fiocco G. and Grams G. (1964) "Observations of the aerosol layer at 20 k by optical radar". J. Atmos. Sci. 21, 323-324.

Grams G.W., Dascher A.J. and Wyman C.M. (1975) "Laser polar nephelometer for airborne measurements of aerosol optical properties". Opt. Eng. 14, 85-90.

Harrison D.N. (1962) "The errors of the Meteorological Office radiosonde, mark 2B. Meteorological Office Scientific Paper No. 15.

Harshvardhan and Cess R.D. (1976) "Stratospheric aerosols: Effect upon atmospheric temperature and global climate". Tellus 28, 1.

Holland A.C. and Gagne G. (1970) "The scattering of polarized light by polydisperse systems of irregular particles". Appl. Opt. 9, 1113-1121.

Hunt G.E. (1971) "A review of computational techniques for analysing the transfer of radiation through a model cloudy atmosphere". J. Quant. Spectros. Radiat. Transfer 11, 655-690.

Irvine W.M. and Peterson F.W. (1970) "Observations of atmospheric extinction from 0.315 to 1.06 microns". J. Atmos. Sci. 27, 62-69.

Lenhard R.W. (1973) "A revised assessment of radiosonde accuracy". Bull. Amer. Met. Soc. 54, 691-693.

Pettifer R.E.W., Jenkins G.J., Healey P.G. and Convery J.H. (1976) "A large coaxial Lidar for elastic inelastic scattering studies of the stratosphere". Optical and Quantum electronics 8, 409-423.

Raschke E., Vonder Haar T.H., Bandeen W.R. and Pasternak M. (1973) "The annual radiation balance of the earth - atmosphere system during 1969-1970 from Nimbus 3 measurements". J. Atmos. Sci 30, 341-364.

Russell P.B., Viezee W., Hake R.D. Jr and Collis R.T.H. (1975) "Lidar observations of the stratospheric aerosol: summary of results and a calibration error assessment". Proceedings Fourth Conference on the Climatic Impact Assessment Program (CIAP), Cambridge, Mass 4-7 February, US Dept. of Transportation.

Russell P.B., Viezee W., Hake R.D. Jr and Collis R.T.H. (1976) "Lidar observations of the stratospheric aerosol : California, October 1972 to March 1974". Quart. J. R. Met. Soc. 102, 675-695.

Toon O.B. and Pollack J.B. (1976) "A global average model of atmospheric aerosols for radiative transfer calculations". J. Appl. Met. 15, 225-246.

Valley S.L. (editor) (1965) "Handbook of Geophysics and Space Environments". McGraw-Hill, New York.

Table 1.

Definition of symbols used in Section 1

z	Altitude variable.
δz	Altitude increment.
z'	Altitude at which aerosol assumed to be absent.
z_1	Lowest altitude at which lidar signal analysed.
E	Receiver system efficiency.
q_0	Atmospheric transmission between ground and z_1.
$q(z)$	Atmospheric transmission between z_1 and z.
P_0	Number of photons transmitted.
$P(z)$	Number of photons received from altitude z.
f_m	Molecular backscatter coefficient.
f_p	Aerosol backscatter coefficient.
$R(z)$	Scattering ratio at altitude z.
R_{MAX}	Maximum value of $R(z)$ in a profile.

Table 2

Contributions to the uncertainties in the scattering ratio

(values are estimated standard deviations in percent)

Altitude (km)	Radiosonde number density errors	Atmospheric transmission errors	Photon Counting errors		Error in the Scattering Ratio	
			465 nm	605 nm	465 nm	605 nm
11	1	0	0.4	0.2	1	1
21	1	0.5	1.5	0.8	2	1.5
29	1	1	4	2.5	4.5	3

Table 3.

Dependence of the derived quantities on the assumed size distribution function, for a refractive index of 1.5-0.001 i.

Size distribution function		Backscatter coefficient* f_p 10^{-9} m^{-1} sr^{-1}		Ratio of solar optical depth to integrated particulate backscatter sr		Ratio of predicted reduction in surface temperature to integrated particulate backscatter ^{o}K sr	
γ	r_c (μm)	λ = 465 nm	λ = 605 nm	465	605	465	605
† 1	0.1	6.689	3.973	25.9	43.5	825	1390
0.7	0.06	3.939	2.409	25.2	41.2	814	1330
0.4	0.025	4.120	2.847	19.3	28.0	617	892
0.3	0.007	0.550	0.369	22.6	33.7	748	1120
0.2	0.005	7.245	6.361	15.5	17.7	471	536

* For a number density of 1 cm^{-3} in the radius range 0.01 to 2 μm.

† This is the Haze H size distribution function (see text).

Table 4.

Error Analysis for the two-wavelength experiment

$R_{605}(z)$	$P_{605}(z)/P_{465}(z)$	Percentage errors required in measured quantities for 100 per cent error in the derived optical depth.	
		$P_{605}(z)$	$\frac{P_{o\,605}}{P_{o\,465}}$, $\frac{E_{605}}{E_{465}}$, $\frac{q^2_{o\,605}}{q^2_{o\,465}}$
1.1	1.56	1.5	1
1.2	1.61	3	2
1.3	1.66	4	3
1.5	1.74	5.5	4
2.0	1.89	6.5	5

Table 5.

Analysis of two-wavelength data for 465 nm (23-24 November 1976) and 605 nm (22-23 November 1976)

Height (km)	465 nm			605 nm			$\frac{f_{p\,465}}{f_{p\,605}}$
	R(z)	Number Density (10^{23} m^{-3})	f_p (10^{-9} m^{-1} sr^{-1})	R(z)	Number Density (10^{23} m^{-3})	f_p (10^{-9} m^{-1} sr^{-1})	
17	1.060	29.3	17.5	1.032	29.6	3.3	5
19	1.074	21.3	15.7	1.046	21.5	3.4	5
21	1.083	15.3	12.7	1.041	15.5	2.2	6
23	1.044	10.9	4.8	1.010	11.2	0.4	12
25	1.045	7.8	3.5	1.018	8.0	0.5	7

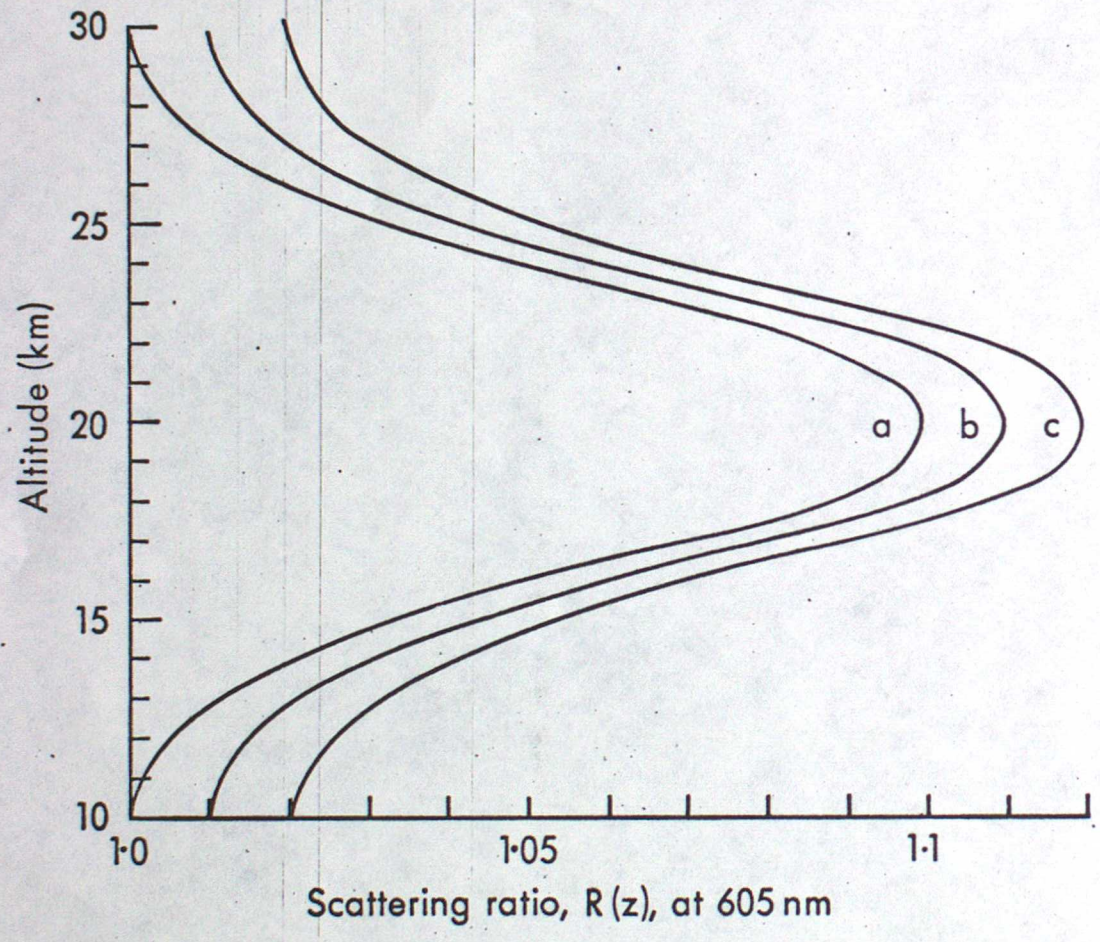

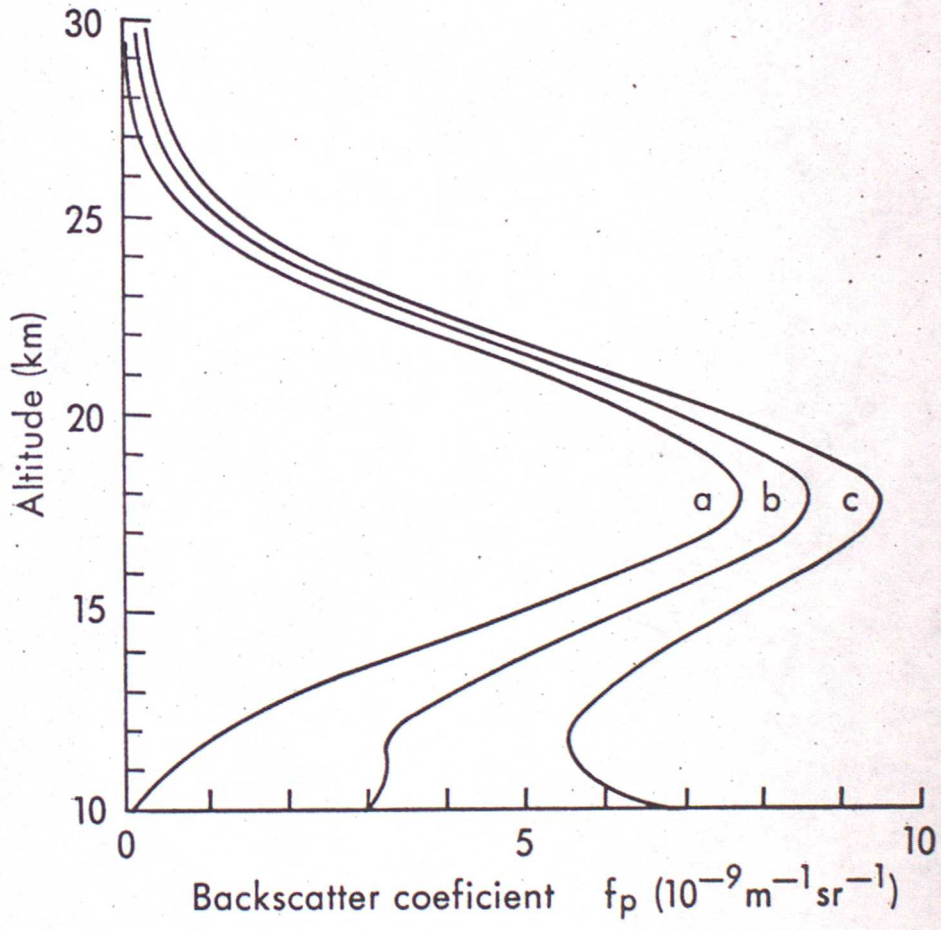

Fig. 1: Theoretical scattering ratio and aerosol backscatter coefficient profiles. Underestimates by 10 per cent and by 20 per cent of (R_{max}-1) at every level transform the profile (a) to profiles (b) and (c), respectively. The effect on the derived aerosol backscatter coefficient is also shown.

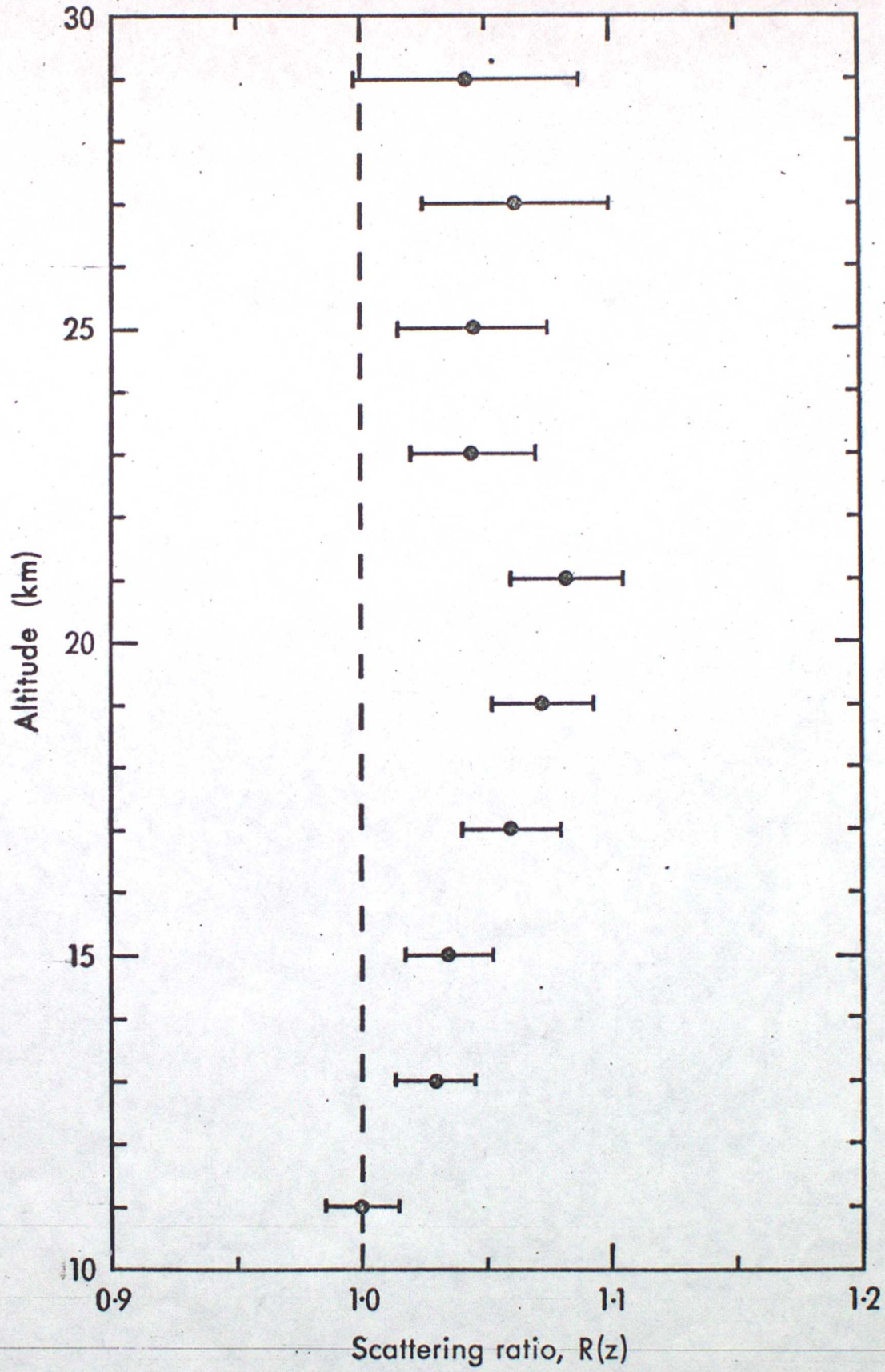

Fig. 2: Scattering ratio profile observed at 465nm on the night of 23/24 November 1976. Error bars are one standard deviation in length. The 'clean-air' normalisation level is 11km.

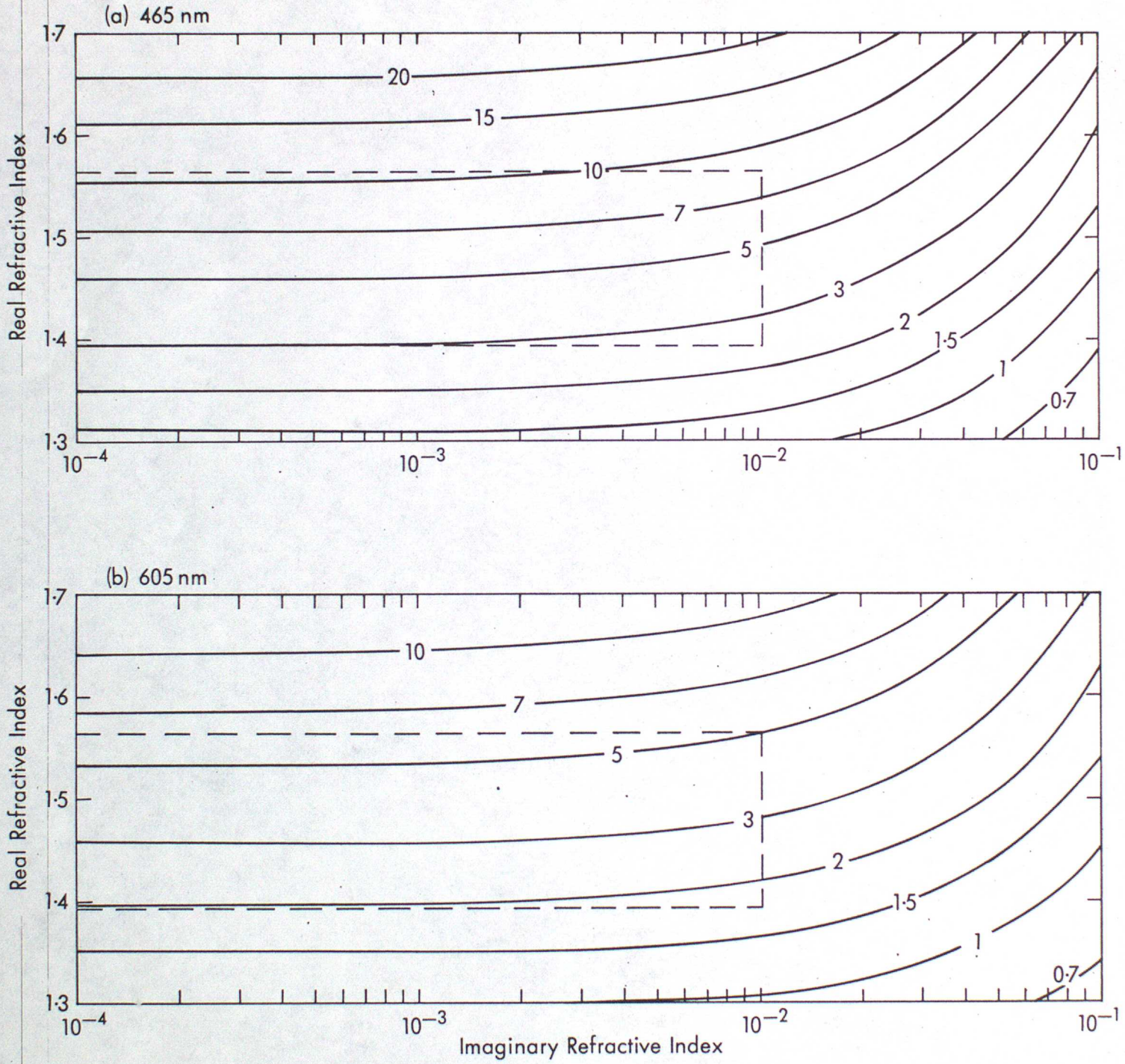

Fig. 3: Backscatter coefficient $f_p(10^{-9}m^{-1}sr^{-1})$, as a function of the real and imaginary parts of the assumed aerosol refractive index at (a) 465 nm and (b) 605 nm, for the Haze H size distribution function with 1 particle per cm^3 in the radius interval 0.01-2 μm.

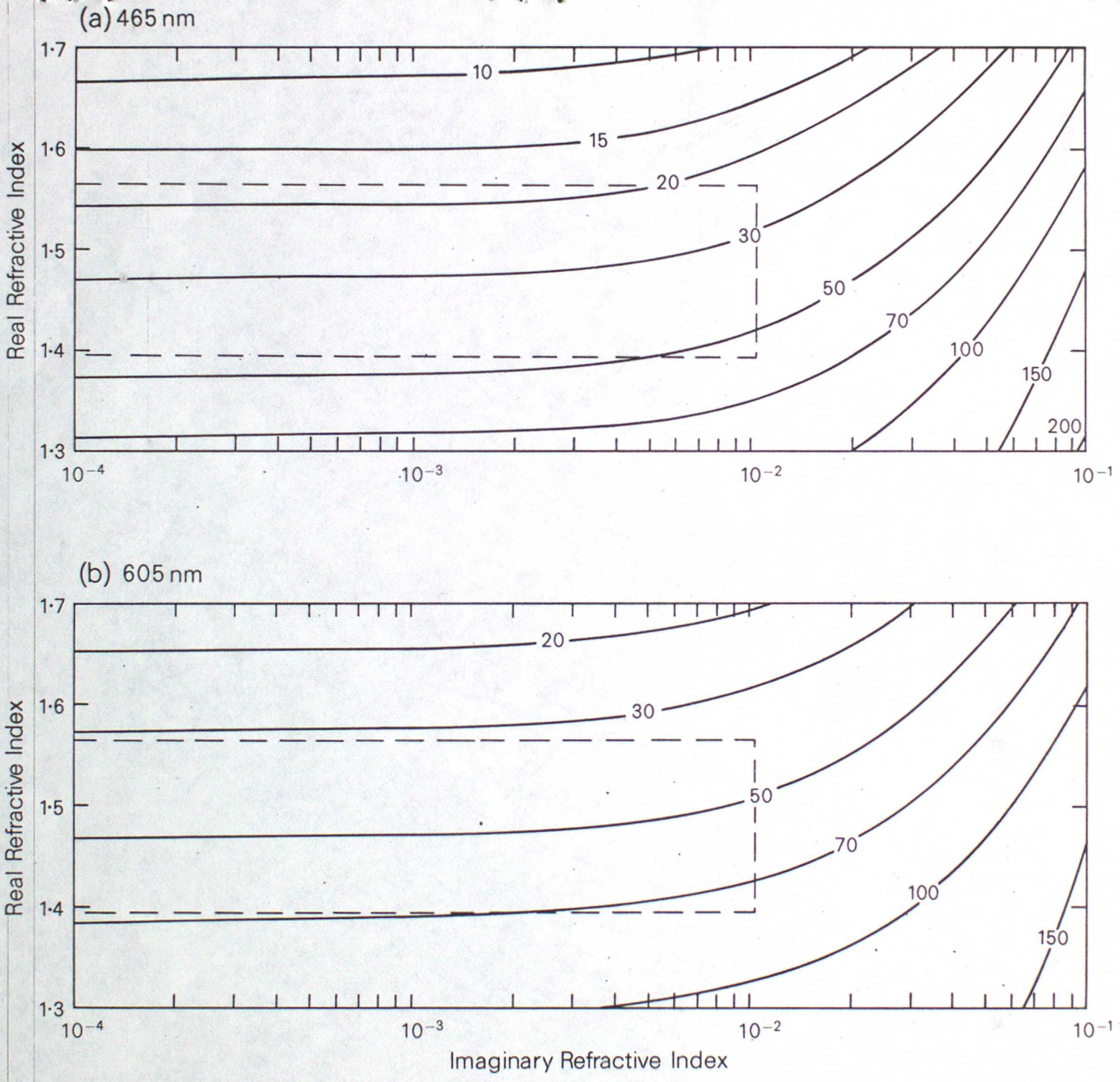

Fig. 4: The ratio of solar optical depth τ to integrated particulate backscatter, (sr), as a function of the real and imaginary parts of the assumed aerosol refractive index, at (a) 465 nm and (b) 605 nm.

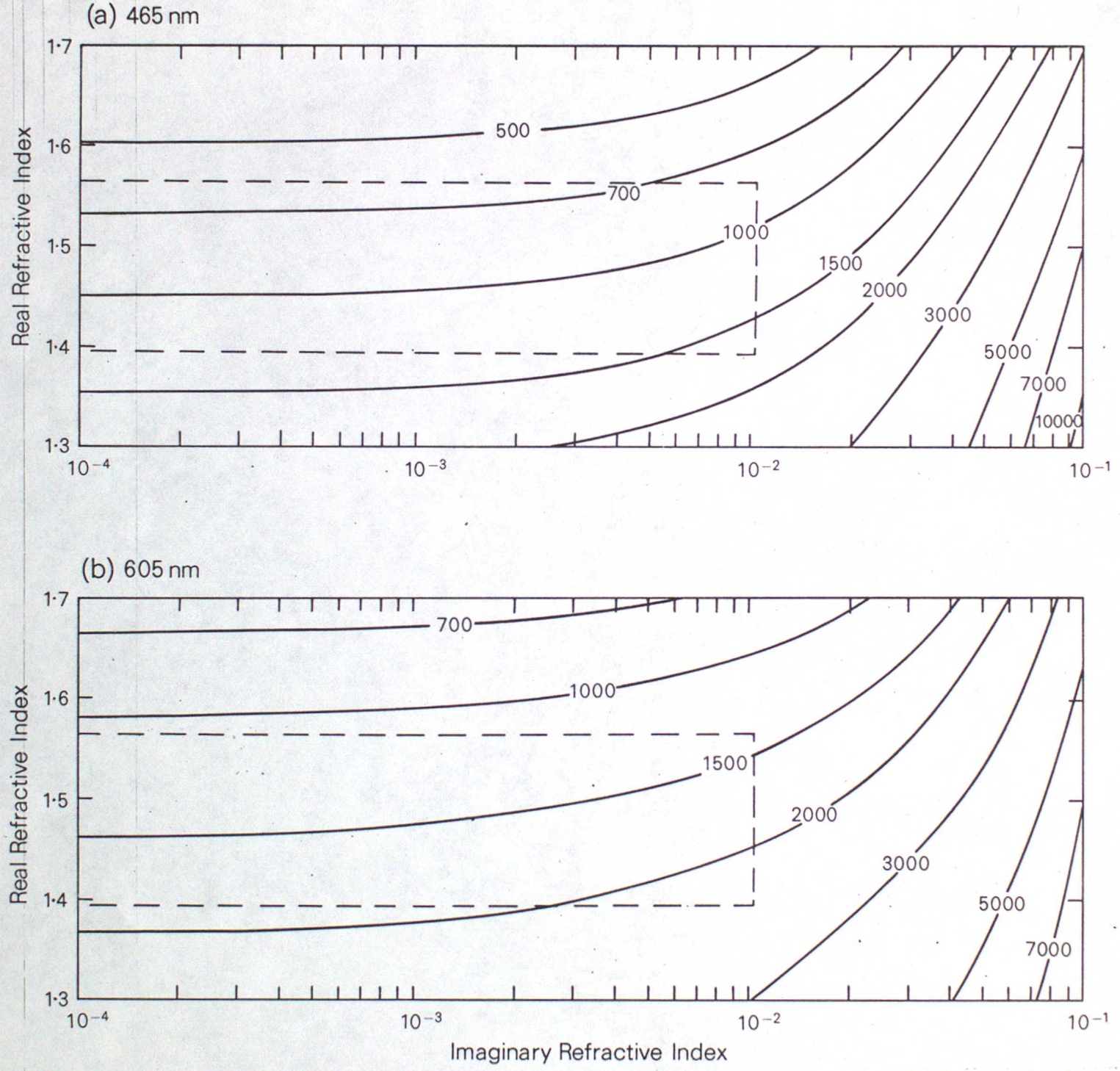

Fig. 5: The ratio of the predicted reduction in surface temperature for a global stratospheric aerosol layer ΔT_S to integrated particulate backscatter, ($^{\circ}$Ksr), as a function of the real and imaginary parts of the assumed aerosol refractive index, for the Haze H size distribution function, at (a) 465 nm and (b) 605 nm

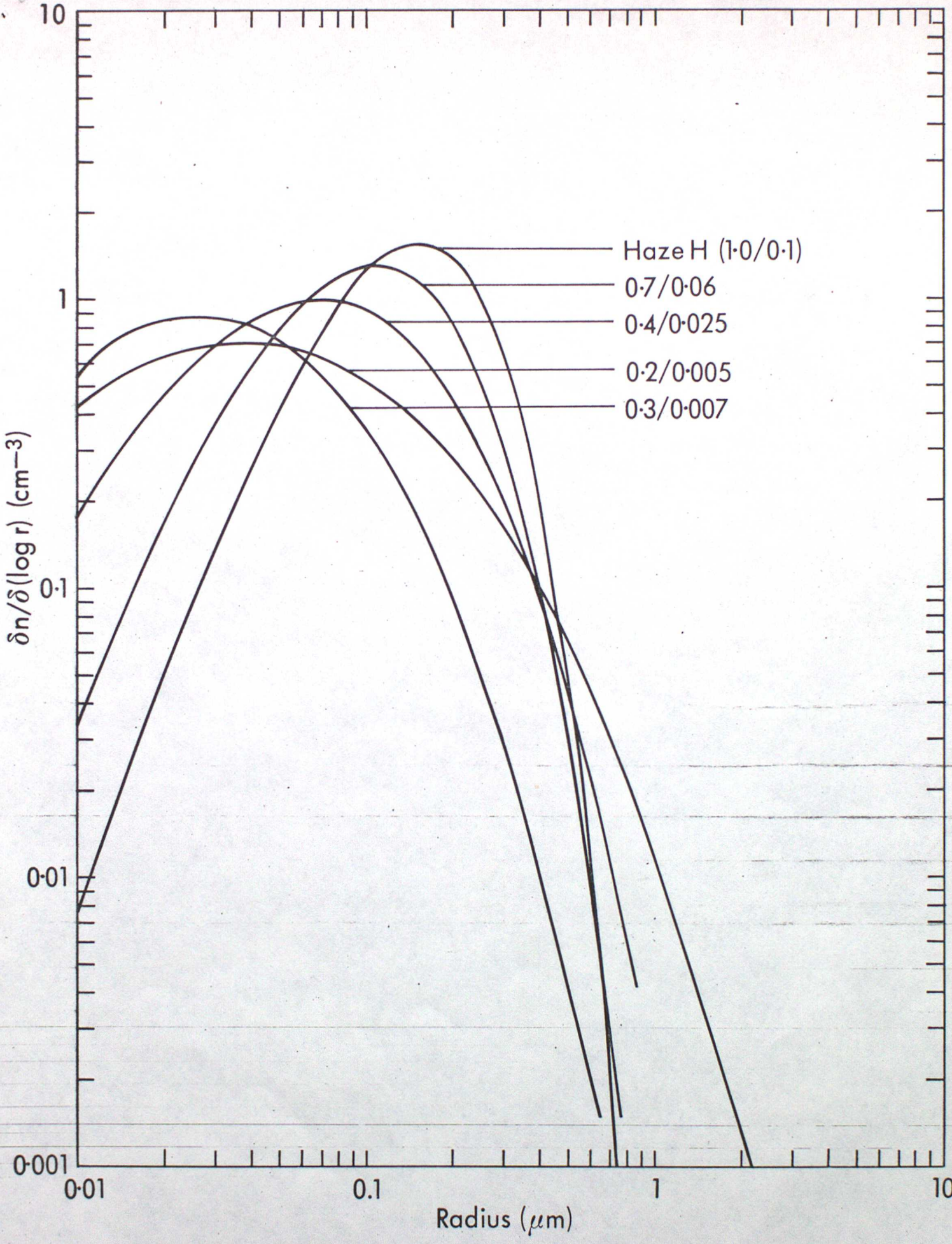

Fig. 6: Size distribution functions used. The values of γ and r_c (see text) are indicated for each function.

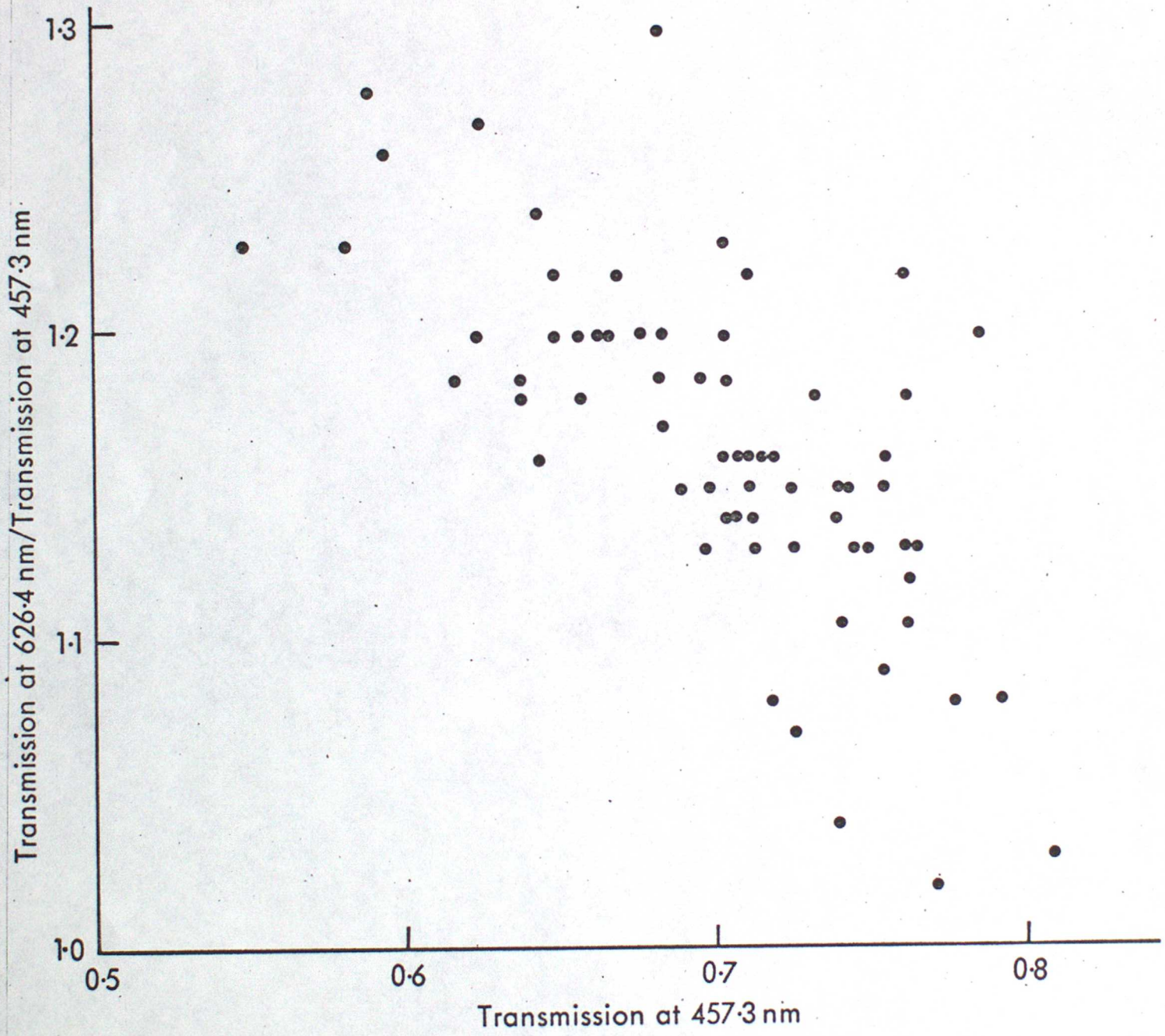

Fig. 7: The ratio of the vertically measured atmospheric transmission at 626.4 nm to that at 457.3 nm, as a function of the latter. Note the dependence of the ratio on transmission. Data taken from Irvine and Peterson (1970).

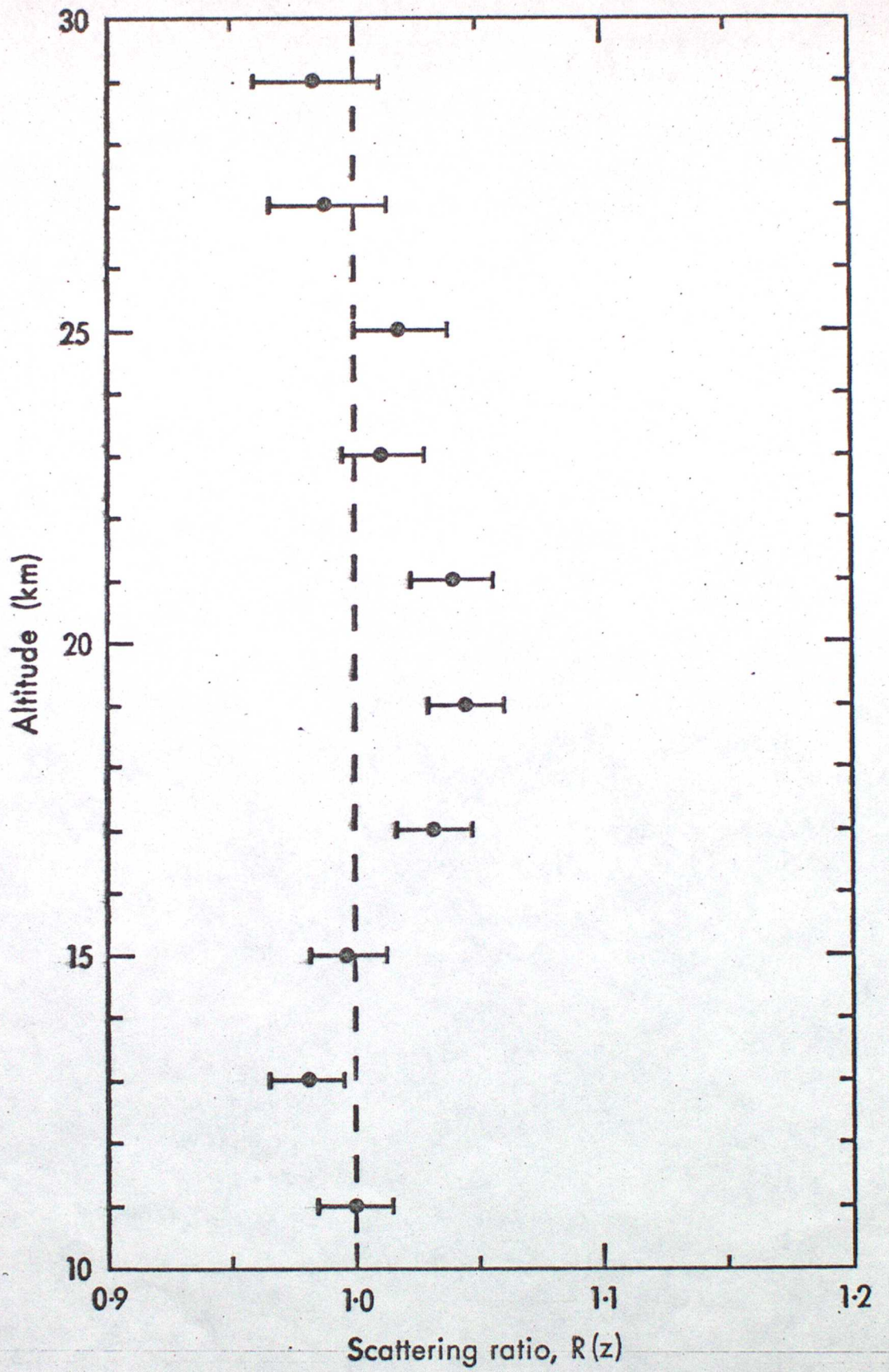

Fig. 8: Scattering ratio profile observed at 605nm on the night of 22/23 November 1976. Error bars are one standard deviation in length. The 'clean-air' normalisation level is 11 km.

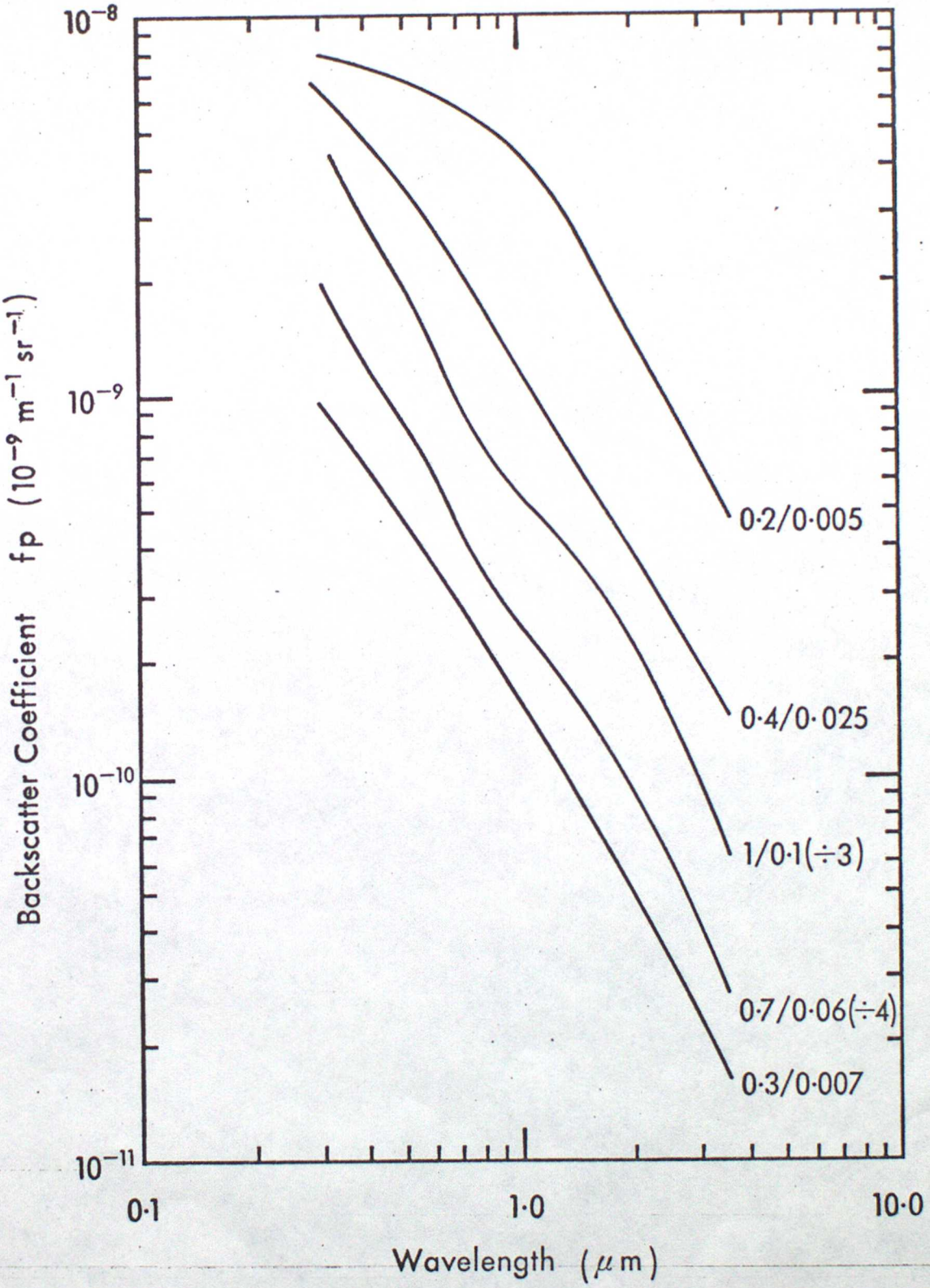

Fig. 9: Wavelength dependence of the aerosol backscatter coefficient f_p, for the model size distribution functions. The values of γ and r_c (see text) are indicated. Two curves have been displaced vertically for the sake of clarity.